ACS OMEGA

Open Access

http://pubs.acs.org/journal/acsodf

Article

A Simple Method to Determine Diffusion Coefficients in Soft Hydrogels for Drug Delivery and Biomedical Applications

Ayomide J. Adeoye and Eva de Alba*

Cite This: *ACS Omega* 2025, 10, 10852−10865

Read Online

ACCESS | Metrics & More | Article Recommendations | Supporting Information

ABSTRACT: Biomedical applications of hydrogels are rapidly increasing due to their special properties including high water absorption capacity, viscoelasticity, swelling capability, and responsiveness to environmental physical or chemical stimuli. Two major biomedical applications of hydrogels include drug delivery and tissue engineering. Knowledge of the diffusion or degree of penetration of particles in hydrogels is key to designing specific functions such as controlled release in drug delivery systems and nutrient accessibility in tissue engineering platforms. Experimental determination of solute penetration and diffusivity can be challenging depending on several factors such as the hydrogelation process, the hydrogel characteristics, and the type of diffusing particle. We describe here a simple method that uses fluorescence intensity measurements obtained with a microplate reader to determine the concentration of diffusing particles at different penetration distances in soft hydrogels. We have analyzed the diffusion behavior of three fluorescent particles of different chemical natures and various molecular weights (fluorescein and the proteins mNeonGreen and fluorophore-labeled bovine serum albumin) in agarose hydrogels of low percentages (0.05−0.2%). The diffusion coefficients were obtained by fitting the experimental data to a one-dimensional diffusion model. A good agreement between our results and previously reported diffusion coefficients of the studied particles validates our method. We demonstrate the method's capability to adapt to hydrogels of different stiffnesses and solutes of various sizes and characteristics. In addition, the combination of hydrogel sectioning with multiple simultaneous measurements in a microplate reader shows the simplicity of the experimental procedure. Finally, our data indicate the method's sensitivity to variations in diffusion conditions, which is highly relevant to studying interactions between solutes and hydrogels designed for controlled release by determining differences in penetration distances.

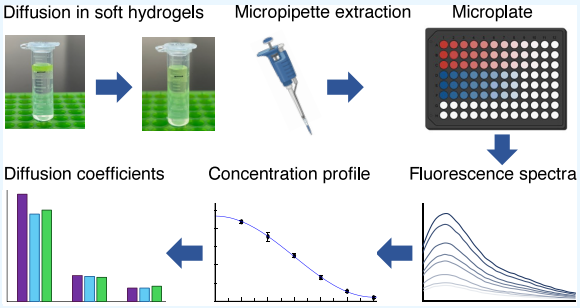

INTRODUCTION

Hydrogels are three-dimensional polymer networks capable of retaining large amounts of aqueous solutions. Several hydrogel properties, such as polymer composition, hydrogel shape and size, porosity, and viscoelasticity can be controlled or modulated. Thus, hydrogels are versatile platforms and scaffolds for diverse applications in the food industry, agriculture, and biomedicine.[1,2] Recently, significant research efforts have focused on hydrogels with functions in pharmacology and medicine.[3,4] Hydrogels have been designed to carry and deliver different drugs including proteins and other biologics.[5−7] For this purpose, the hydrogel responsiveness to environmental conditions such as mechanical forces, pH, temperature, and exposure to light[8−10] is a key factor impacting the time of the drug's sustained release. Certain hydrogel designs help control the spatiotemporal release of therapeutics.[11−14] Furthermore, the hydrogel network provides stability and acts as a protective barrier from degradation.

In addition, hydrogels are used as scaffolds in tissue engineering for regenerative medicine, wound healing, and prosthesis fabrication.[15−21] These applications include repair and growth of bone, cartilage, vascular, skin, and cornea tissues, among others.[16] The hydrogels serve as matrices carrying cells, chemicals, and biologics required for cell growth, adhesion, and migration. Particularly for avascular tissue regeneration, essential biomolecules such as growth factors must be delivered directly into the tissue microenvironment.[16] Thus, hydrogels for tissue repair and regeneration must have the required mechanical properties together with the capability to carry and release certain biomolecules.[16−18]

The diffusion of nutrients, oxygen, drugs, biologics, liposomes,[22] nanoparticles, and essential biomolecules such as growth factors, is key to the success of hydrogel applications. Therefore, advances in the knowledge of the factors controlling particle diffusion in hydrogels and experimental methods to study diffusion processes are highly relevant to hydrogel

Received: July 30, 2024
Revised: February 18, 2025
Accepted: February 21, 2025
Published: March 11, 2025

design. Several factors are typically considered to impact the diffusion of solutes in hydrogels,[23] such as the interactions between the hydrogel network and the solute,[24] obstacles to solute transport by the hydrogel matrix,[25] and the potential movement of the solute in empty spaces between molecules.[26] All these considerations are combined in a multiscale model for solute diffusion in hydrogels that provides accurate predictions for the diffusivity of dextran solutes in polyethylene glycol gels.[23] Also, solutes may experience chemical interactions with the hydrogel matrix, such as hydrophobic effects, electrostatic attractions, and repulsions that can affect diffusivity.[27] In such cases, theoretical models to predict diffusion behavior become more complicated.

Experimental methods to study the diffusivity of particles in hydrogels are essential to design controlled release applications and make predictions on the time required for nutrients to reach the tissues or cells that grow in or adhere to a hydrogel matrix.[28] Diffusion coefficients in gels have been measured using Nuclear Magnetic Resonance spectroscopy (NMR),[29,30] infrared spectroscopy,[31] light refraction,[32] holographic interferometry,[33] and fluorescence microscopy. The latter typically involves total internal reflection fluorescence[34] and fluorescence recovery after photobleaching.[35] Most methods rely on the presence of steady-state or nonsteady-state concentration gradients created by the diffusing particle or solute. The length- and/or time-dependent concentration gradient profile created by diffusion is studied using different techniques. Some diffusion studies monitor the concentration of the particles that have diffused from the hydrogel to a solution in contact with it, and less commonly diffusivity is analyzed in the hydrogel body. In the latter case, the hydrogel material should not interfere with the measurement reporting the presence of the solute. Methods to determine diffusion coefficients by fluorescence recovery after photobleaching or fluorescent intensity, typically require the use of microscopes. Thus, the hydrogel dimensions are restricted to fit the microscope slides, capillaries, or microfluidic devices. Methods involving NMR need extensive user training and expensive magnets. In most cases, diffusivity studies are done for individual hydrogels, significantly extending the time dedicated to the experimental measurements.

Hydrogels made of natural materials are typically preferred in biomedical applications due to increased biocompatibility. Agarose, for instance, is a natural polysaccharide extracted from seaweed, specifically from red algae, that can form stable hydrogels.[36,37] These hydrogels are prepared by heating agarose solutions typically to 90−100 °C to disrupt the hydrogen bonds connecting the polysaccharide chains, which dissolve and form clear solutions. A subsequent cooling process to ∼30 °C leads to the formation of intertwined bundles of coiled coils of double helices as structural units.[38] Agarose hydrogels have multiple applications that include electrophoresis for the separation of biomolecules in the presence of an electric field, as a basic material in matrices used for size exclusion chromatography, as well as in drug delivery and tissue engineering.[36,38−40] In addition, agarose can be modified chemically to produce low-melting agarose leading to improved sieving properties and better separation of biomolecules such as DNA.[36]

Agarose presents several advantages in drug delivery applications compared to other polysaccharide-based materials such as chitosan or cellulose.[41] Agarose can be easily dissolved, and the average pore size can be controlled by the agarose percentage, which has a key impact on solute diffusivity and, thus, the control of drug release.[41] In addition to pore size, potential interactions between the drug and the agarose need to be considered in diffusion studies as positively charged species tend to engage in electrostatic interactions with the polysaccharides; however, these interactions can be shielded by increasing the ionic strength of the solution.[42] In addition, the tunable mechanical properties of agarose hydrogels and their biocompatibility facilitate cell proliferation, adhesion, and migration thus favoring their applications in tissue engineering and regenerative medicine. For example, agarose hydrogels have been used in cartilage engineering,[39] as well as axonal,[43] bone,[44] and skin[45] regeneration. Hybrid hydrogels composed of agarose and gallic acid have been reported to expedite wound healing and diminish inflammation in vivo.[46]

Overall, the application of agarose hydrogels in drug delivery and tissue engineering requires understanding and determining solute diffusivity. Protein diffusion in agarose hydrogels has been determined by measuring changes in refractive index resulting in a range of diffusion coefficients of $0.49-0.82 \times 10^{-4}$ mm^2/s for Bovine Serum Albumin (BSA) and $1.1-1.5 \times 10^{-4}$ mm^2/s for lysozyme at 37 °C in agarose percentages in the 0.5−3.0% range.[32] This work demonstrates that protein diffusion coefficients increase at lower agarose percentages and lower molecule weight of the protein and shows that BSA's diffusivity decreases with temperature. Another study, employing microfluidics and UV-based imaging techniques, determined a diffusion coefficient of lysozyme of $0.80 \pm 0.04 \times 10^{-4}$ mm^2/s in 1.5% low-melting agarose and $1.14 \pm 0.02 \times 10^{-4}$ mm^2/s in 0.5% unmodified agarose.[47]

The method described here is based on determining the concentration gradient of diffusing particles inside hydrogels by analyzing hydrogel sections using fluorescence spectroscopy with a microplate reader. Hydrogel sectioning has been used previously to obtain diffusion coefficients;[48] however, the diffusing particles are typically released to a solution from the gel slab, or the hydrogel is dissolved to obtain measurements in homogeneous solutions.[49,50] These procedures can lead to unwanted experimental errors or damage delicate diffusing particles such as proteins. Our method has the following advantages: 1) no specific hydrogel dimensions are required, in contrast to methods that need the hydrogel to fit vessels or cells used for measurements, such as cuvettes for spectrophotometers, or microfluidic devices and slides for microscopes; 2) the measurements are done directly in hydrogel sections, thus the diffusing particle does not have to be extracted nor does the hydrogel need to be dissolved; 3) the diffusion of particles of different chemical nature such as organic dyes and proteins of a broad size range can be studied; 4) a large number of wells in the microplate permits multiple and simultaneous measurements; 5) the chemical composition of the hydrogel is not a limiting factor if it is not fluorescent, in contrast to methods using absorbance spectroscopy that might not be suited for protein-based hydrogels; 6) the hydrogel viscoelastic properties are not limiting factors; hydrogel slicing is not required thus broadening applications for soft hydrogels.

RESULTS

Method Description. The method presented here is based on fluorescence spectroscopy to measure the concentration of fluorescent particles as a function of penetration distance after diffusing in hydrogels for fixed times. As proof of concept, we prepared agarose hydrogels of different percentages to test the

https://doi.org/10.1021/acsomega.4c06984
ACS Omega 2025, 10, 10852−10865

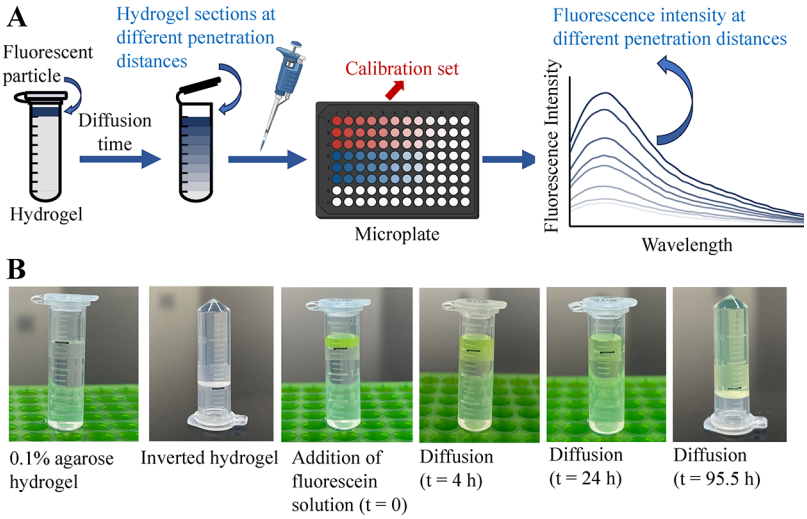

Figure 1. Fluorescence spectroscopy using microplates to determine particle concentration as a function of penetration distance after diffusion in hydrogels. (A) Schematic representation of the method's procedure, showing the calibration set (red) and the hydrogel sections (blue) in the microplate for three independent experiments. (B) Diffusion of a highly concentrated fluorescein solution (30 μM) in an agarose hydrogel showing the relevant green color and its diffusion as a function of time (h = hour) and penetration distance. The hydrogel below the black mark in the last panel to the right shows the swollen hydrogel.

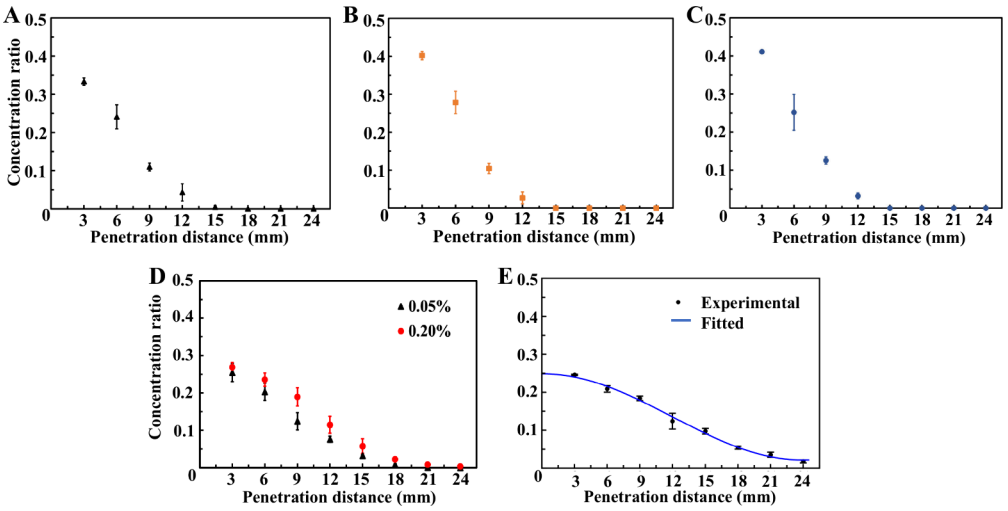

Figure 2. Diffusion of fluorescein in agarose hydrogels. (A–C) Concentration ratios (C_i/C_0) of fluorescein as a function of penetration distance at 4 h of diffusion in 0.05%, 0.1%, and 0.2% agarose. (D) 14 h diffusion in 0.05% and 0.2% agarose. (E) 24 h diffusion in 0.05% agarose and fitting to a 1D diffusion model (blue line). All values are averages of three independent experiments, and error bars indicate the standard deviations.

potential effects of pore sizes in diffusion. We chose agarose percentages of 0.05%, 0.1%, and 0.2% to test our method in soft hydrogels that cannot be sliced. These percentages are significantly smaller than those typically used for separations of DNA and other molecules (~0.5%–2.0%).[36] Solutes with large differences in hydrodynamic radii were analyzed to assess the impact of particle size on diffusion. Specifically, solutions of fluorescein (0.3 kDa), and the proteins mNeonGreen (27 kDa) and fluorophore-labeled bovine serum albumin (BSA, 68 kDa) were prepared as described in the Methods Section.

A schematic representation of the method is depicted in Figure 1. Agarose hydrogels of different percentages were formed in microcentrifuge tubes. A fixed volume of the fluorescent particle solution at a known concentration (C_0) was placed on the surface of the agarose hydrogel and allowed to diffuse at controlled times. Sections of the hydrogel need to be extracted and analyzed to determine the concentration of the fluorescent particle as a function of penetration distance. Hydrogel slicing is not possible due to the low stiffness resulting from the small agarose percentages. Thus, hydrogel sections were extracted from top to bottom at fixed distances with micropipettes and wide bore tips (Figure 1). Due to the soft nature of the hydrogels, extractions of hydrogel sections at very small lengths by manual pipetting in the dark are difficult and can lead to errors in the concentration profile. However, we could carefully extract sections every 3 mm to ensure the complete removal of a hydrogel section. The volume of the agarose hydrogels was optimized to allow for sufficient penetration, leading to a concentration profile with at least 8 penetration distance points for an appropriate sampling. Thus, the maximum diffusion distance considered was 24 mm.

After extraction, each hydrogel section was thoroughly mixed by pipetting for 5 s, leading to a uniform particle concentration. To test the potential effects of homogenization

https://doi.org/10.1021/acsomega.4c06984
ACS Omega 2025, 10, 10852–10865

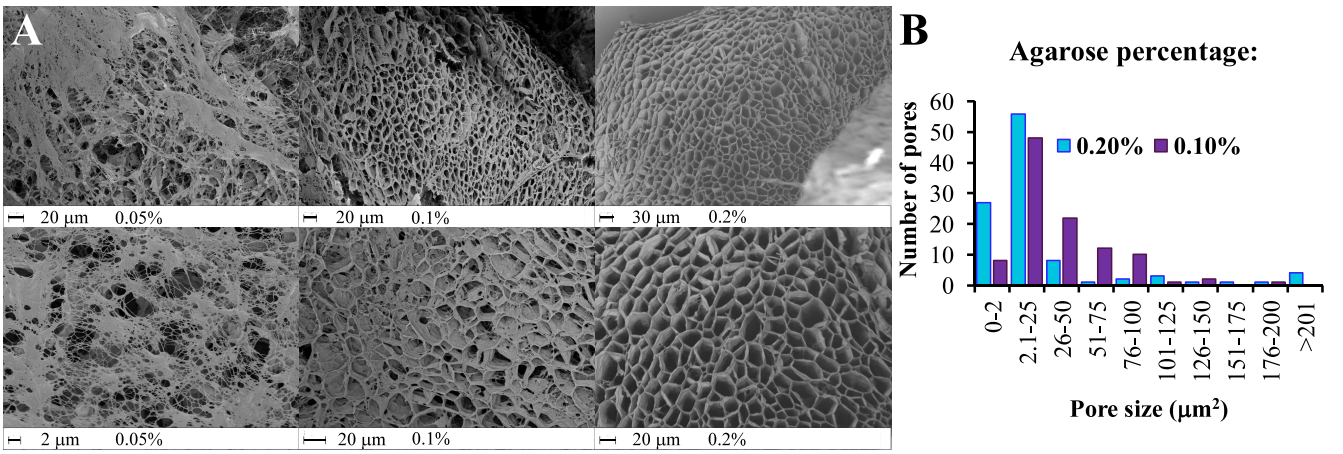

Figure 3. Pore size analysis of low-percentage agarose hydrogels. (A) Different magnifications of representative SEM images of agarose hydrogels (scale bars and percentages are indicated at the bottom of the micrographs). (B) Pore size analysis of the 0.1% and 0.2% hydrogels (N = 100).

time and method on fluorescence intensity and concentration values, we performed 4-h fluorescein diffusion experiments in 0.05%, 0.1%, and 0.2% agarose hydrogels and homogenized different sections by pipetting for 5 s, 15 s, and low-speed vortexing for 15 s. No significant variations were observed in fluorescence intensity or particle concentration values at the different homogenization times and methods (Figure S1). These results indicate that vortexing or pipetting for 5 s is sufficient for thorough homogenization.

The homogenized hydrogel sections were placed on microplate wells to obtain with a microplate reader the fluorescence intensity emitted by the particles that penetrated the hydrogel due to diffusion. As a reference, we measured the fluorescence intensity of solutions of each solute at different known concentrations to generate calibration plots (Figure S2). The concentrations of the fluorescent particles in each hydrogel section (C_i) were calculated by extrapolation from the calibration functions (Figure S2). Subsequently, we calculated the concentration ratios (C_i/C_0) to determine the extent of penetration of the fluorescent solutes in the hydrogels under different agarose percentages and diffusion times. The method described here is designed for nonsliceable soft hydrogels; however, it can be easily applied to hydrogels with high cross-linking density, requiring slice extraction. In such cases, the hydrogel slices should be of identical volumes for quantitative analysis. Microplates with flat-bottom wells are ideal for stiff hydrogels, and the slices should preferentially be placed at the center of the well's bottom. We anticipate that the error in determining the volume of the slices will be larger than for soft hydrogels, which allow the use of a micropipette. Microplate readers have been used to detect fluorescence in hydrogels for different purposes.[51,52]

Under the conditions described regarding sampling and hydrogel dimensions, the diffusion experiments ranged from 4 h to 5 days, depending on particle size. Specifically, we performed independent diffusion experiments at different hydrogel percentages and diffusion times of 4, 14, and 24 h for fluorescein; 6, 14, 24, 48 h, and 5 days for mNeonGreen; and 48 h and 5 days for fluorescent BSA.

Solute Penetration Measurements. Diffusion experiments of fluorescein solutions representing the C_i/C_0 ratios as a function of penetration distances are shown in Figure 2. At the same diffusion time of 4 h, fluorescein penetrates more in the 0.05% agarose hydrogel relative to the 0.1% and 0.2% (Figure 2A–C). However, no significant differences were observed for the latter percentages. At a diffusion time of 14 h, fluorescein penetration is more pronounced in 0.05% and 0.2% agarose compared to the data obtained at the shorter diffusion time of 4 h, and the penetration is again higher for the lower agarose percentage (Figure 2D). Finally, fluorescein penetration after 24 h diffusion is larger than at shorter times as expected (Figure 2E).

A pore size analysis of agarose hydrogels with percentages ranging from 0.5% to 3.0% has been reported previously.[53] This work shows an apparent exponential increase in pore size at decreasing agarose percentages with values up to 1200 nm at 0.5% high-melting agarose.[53] To obtain information on pore sizes of agarose hydrogels at 0.05%, 0.1%, and 0.2%, we used SEM (Scanning Electron Microscopy) image analysis. Representative images of the agarose hydrogels at different percentages are shown in Figure 3 together with the corresponding analysis. The pore size analysis shows that the 0.1% agarose hydrogels contain a higher number of larger pores than the 0.2% hydrogels, particularly in the range of 51–100 μm^2 (Figure 3B). No pores were analyzed for the 0.05% agarose hydrogel due to the different morphology, likely resulting from a weaker network unable to sustain the lyophilization process prior to SEM image acquisition. Nonetheless, we expect an analogous trend based on our results and previously reported data.[53] Importantly, the hydrogel average pore size (mesh size) depends on the cross-linking density, such that larger pore sizes correspond to lower cross-linking densities and *vice versa*.[54] Thus, the 0.05% agarose hydrogel with larger pores and lower cross-linking density will pose less resistance to fluorescein penetration, as observed (Figure 2). Due to the exponential behavior of pore size vs agarose percentage,[53] the structural differences between the 0.1% and 0.2% agarose hydrogels might not be as drastic as to lead to significant differences in penetration.

Overall, these data indicate that our method based on the extraction of hydrogel sections and their analysis by fluorescence spectroscopy is suitable for determining the penetration distances of a small dye like fluorescein diffusing in hydrogels. Applying this method, we can identify variations in penetration distances resulting from different agarose percentages and diffusion times.

To test the performance of our method with particles of different chemical compositions and sizes, we carried out

https://doi.org/10.1021/acsomega.4c06984
ACS Omega 2025, 10, 10852–10865

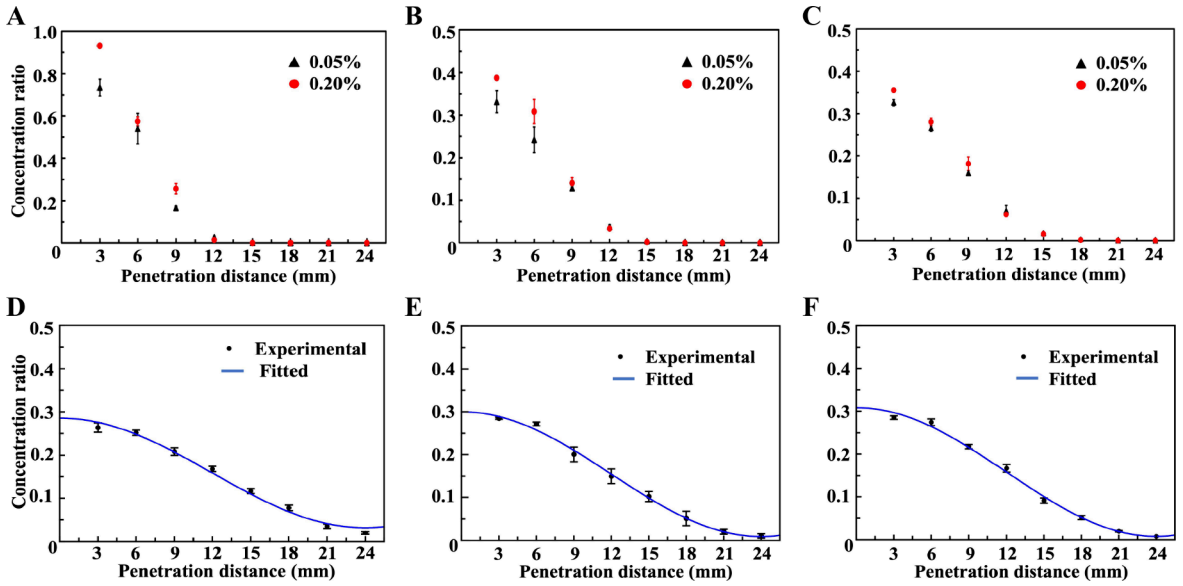

Figure 4. Diffusion of mNeonGreen in agarose hydrogels. (A−C) Concentration ratios (C_i/C_0) of mNeonGreen as a function of penetration distance at 14, 24, and 48 h of diffusion (agarose percentages indicated). (D−F) 5-day diffusion in 0.05%, 0.1%, and 0.2% agarose and fitting to a 1D diffusion model (blue lines). All values are averages of two independent experiments, and error bars indicate the standard deviations.

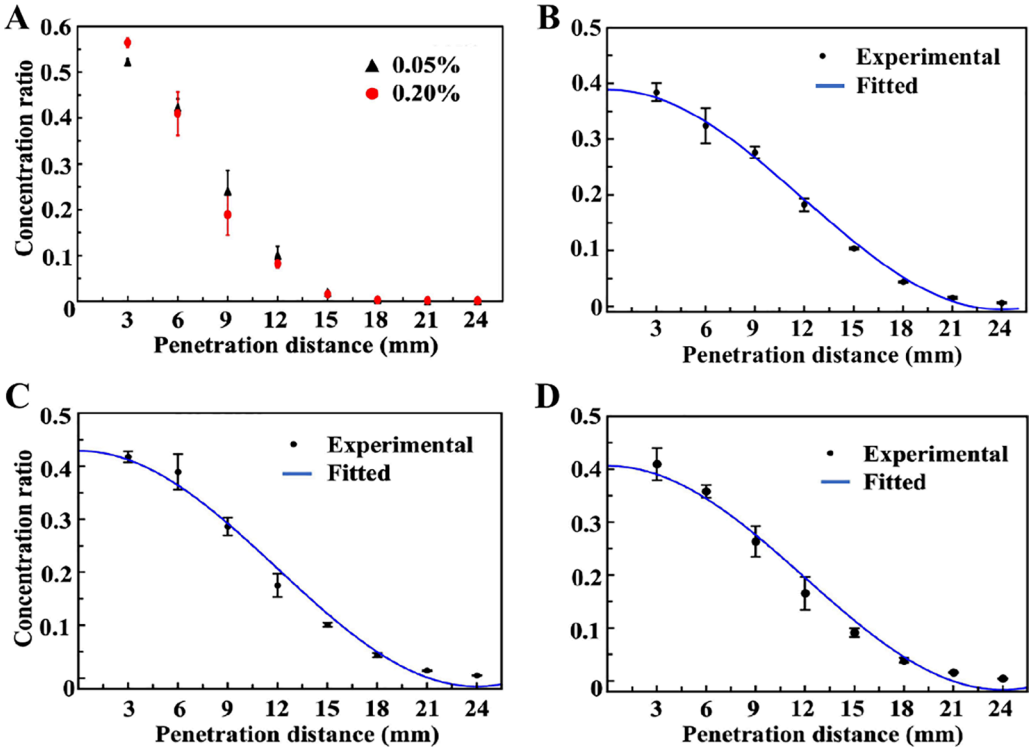

Figure 5. Diffusion of fluorescent BSA in agarose hydrogels. (A) Concentration ratios (C_i/C_0) of fluorescent BSA as a function of penetration distance at 48 h of diffusion (agarose percentages indicated). (B−D) 5-day diffusion in 0.05%, 0.1%, and 0.2% agarose, respectively, and fitting to a 1D diffusion model (blue lines). All values are averages of three independent experiments, and error bars indicate the standard deviations.

analogous experiments on the fluorescent protein mNeonGreen which has a significantly larger molecular weight compared to fluorescein. The diffusion results by comparing the C_i/C_0 ratios at 14, 24, and 48 h indicate that penetration is more pronounced at longer diffusion times (Figure 4A−C). In addition, more penetration is observed at lower percentages of agarose, analogously to the results obtained with fluorescein. The protein diffuses much slower than fluorescein at the same diffusion times of 14 and 24 h (Figure 2D,E and Figure 4A,B). In fact, mNeonGreen barely penetrates the hydrogel at 6 h, showing C_i/C_0 ratios of ∼0.8 and ∼0.55 at 3- and 6 mm penetration distances, respectively (Figure S2D). At a longer diffusion time (5 days), slight differences in protein penetration with agarose percentage were only observed for 0.05% compared to 0.1% or 0.2% agarose (Figure 4D−F).

Finally, we have analyzed the diffusion behavior of fluorescent BSA with a significantly larger molecular mass relative to fluorescein and mNeonGreen. Due to the larger

https://doi.org/10.1021/acsomega.4c06984
ACS Omega 2025, 10, 10852−10865

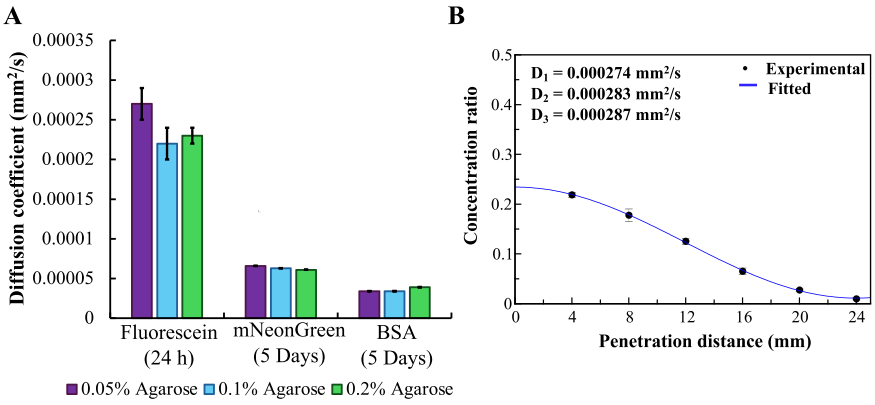

Figure 6. Diffusion coefficients and discretization effects. (A) Bar chart of D values obtained from fitting the experimental diffusion data to eq 1. The name of the fluorescent particle and agarose percentage for hydrogelation are indicated in the plot. (B) Concentration ratios as a function of penetration distance of the diffusion of fluorescein in 0.05% agarose with hydrogel sections extracted every 4 mm. The three individual D values are indicated in the inset. The bar heights in panel (A) and C_i/C_0 ratios in panel (B) represent averages, and the error bars indicate standard deviations from two (mNeonGreen) and three (fluorescein and BSA) independent experiments.

Table 1. Comparison of Obtained and Reported Diffusion Coefficients (D)

Particles	[a]R_H (nm)	[b]MW (kDa)	Reported D ($mm^2/s \times 10^{-4}$)	Obtained D ($mm^2/s \times 10^{-4}$)
Fluorescein	0.5[57]	0.3	$D_{2.7\%\ hydroxyethyl\ cellulose\ gel} = 2.69 \pm 0.03$[58] $D_{water} = 4.86 \pm 0.03$[58]	**Fluorescein at 24 h:** $D_{0.05\%\ agarose} = 2.7 \pm 0.2$ $D_{0.1\%\ agarose} = 2.2 \pm 0.2$ $D_{0.2\%\ agarose} = 2.3 \pm 0.1$
mNeonGreen	2.8[59]	27	Green fluorescent protein in water: $D = 0.87 \pm 0.02$[60]	**mNeonGreen at 5 days:** $D_{0.05\%\ agarose} = 0.659 \pm 0.002$ $D_{0.1\%\ agarose} = 0.63 \pm 0.02$ $D_{0.2\%\ agarose} = 0.61 \pm 0.01$
BSA	7[61]	68	$D_{4\%\ agarose} = 0.498 \pm 0.006$[62] $D_{0.5-3.0\%\ agarose}$: 0.498–0.821[32] [c]$D_{4\%\ agarose}$: 0.23–0.65[63]	**BSA-Dylight 488 at 5 days:** $D_{0.05\%\ agarose} = 0.34 \pm 0.03$ $D_{0.1\%\ agarose} = 0.34 \pm 0.04$ $D_{0.2\%\ agarose} = 0.39 \pm 0.04$

[a]R_h: Hydrodynamic radius. [b]MW: Molecular weight. [c]Determined at different pH values and ionic strengths.

particle size, fluorescent BSA requires longer diffusion times to penetrate the agarose hydrogels (Figure 5). C_i/C_o values comparable to those of fluorescein and mNeonGreen are observed after 48 h of diffusion for fluorescent BSA instead of 4 and 14 h for fluorescein and mNeonGreen, respectively. No significant differences in penetration distances were observed between 0.05% and 0.2% agarose hydrogels.

The method proposed here allows us to determine the concentration of fluorescent particles at different penetration distances after particle diffusion in agarose hydrogels. By extracting hydrogel sections and determining particle concentration with fluorescence spectroscopy in a microplate reader, we can identify differences in diffusion as a function of time, agarose percentage (pore size), and particle size. Specifically, analogous penetrations to those attained by fluorescein after 4 h of diffusion were observed for both proteins, with significantly larger sizes compared to fluorescein, only after several days of diffusion time. This is an expected result as agarose hydrogels are commonly used to separate molecules based on size in electrophoresis. Larger molecules travel shorter distances in agarose hydrogels compared to smaller molecules because the hydrogel network acts as a sieve, causing friction and hindering molecular displacement.[40] In addition, increased particle penetration is observed at lower agarose percentages, particularly when comparing data obtained at 0.05% and 0.2% for the shorter diffusion times. These results are also expected as lower agarose percentages lead to increased pore sizes and thus lower cross-linking density. Overall, these positive results led us to attempt to determine particle diffusion coefficients.

Diffusion Coefficient Determination. Several assumptions were made to determine the diffusion coefficient (D) of fluorescein, mNeonGreen, and BSA in the agarose hydrogels: 1) diffusion is the only mechanism for the mass transfer phenomenon that occurs when the solutions of fluorescent solutes traverse the hydrogels (i.e., the solutes do not interact with the hydrogel); 2) a diffusive front leads to the mass flux in one-dimension occurring along the normal of the hydrogel's top surface (Figure 1B); 3) diffusion is isotropic; 4) the diffusion coefficient is constant; 5) the boundary conditions include an impermeable surface (i.e., no flux occurs at the top surface of the hydrogel) and a finite length of the hydrogel leading to a homogeneous concentration at infinite diffusion times. Under these assumptions and applying Fick's first and second laws of diffusion, eq 1 is derived following previously described mathematical methods[55,56] to determine D.

$$\frac{C(x,t)}{C_0} = \sum_{m=1}^{\infty} B_m \cos\left(\frac{\pi m x}{L}\right) e^{-\pi^2 m^2 D t / L^2} + C_f \quad (1)$$

Where $C(x, t) = C_i$ is the concentration of the fluorescent particle at different penetration distances (x) and diffusion times (t); C_0 is the initial concentration of the fluorescent

https://doi.org/10.1021/acsomega.4c06984
ACS Omega 2025, 10, 10852−10865

particle; B_m is a coefficient that depends on the concentration distribution at the first hydrogel section; C_f is the homogeneous concentration reached at diffusion times longer than the expected diffusive range; L is the hydrogel length after swelling; D is the diffusion coefficient. Because we are considering a diffusive front, the dominant mode is $m = 1$ and other values of m were not considered.[56]

The experimental C_i/C_0 values as a function of penetration distances were fitted to eq 1 at diffusion times of 24 h for fluorescein and 5 days for mNeonGreen and fluorescent BSA (Figures 2E, 4D−F, and 5B−D). The D values were obtained from the fittings of two to three independent experiments (Figure 6A). No significant differences are observed in the D values for mNeonGreen and BSA at different agarose percentages; however, fluorescein's D is slightly higher in the 0.05% hydrogel. Generally, we can consider that the pore sizes are sufficiently large in all agarose percentages (Figure 3) thus leading to similar diffusion coefficients.

To test the performance of our method, we have compared the D values shown in Figure 6A with previously reported values of the same or similar size particles determined under different conditions (Table 1). For example, fluorescein's D value in hydroxyethyl cellulose gel is similar to the values obtained with our method at the different agarose percentages. The diffusion coefficient of green fluorescent protein in water, with a molecular mass of 27 kDa close to that of mNeonGreen, is higher than our values in hydrogels as expected. The D values of BSA at agarose percentages higher than those used in this study vary depending on pH and ionic strength in the $0.23-0.82 \times 10^{-4}$ mm^2/s range (Table 1). The diffusion coefficient for BSA obtained with our method falls within this range. Overall, there is good agreement with previously reported D values, thus validating the method presented here.

Finally, we investigated the potential effects of discretization in determining the diffusion coefficients. For this purpose, we performed three independent experiments of 24-h diffusion of fluorescein at 0.05% agarose extracting hydrogel sections every 4 mm. The diffusion data were fitted to eq 1 (Figure 6B). The D values obtained are very similar to those shown in Figure 6A and Table 1. These results indicate that discretization does not influence the diffusion coefficients obtained with this method.

DISCUSSION

Hydrogels can be biocompatible carriers for drug delivery, tissue engineering scaffolds, and platforms for implants and prostheses. The hydrogel three-dimensional polymeric network restricts access to natural degrading factors in the human body such as proteases and other enzymes, thus protecting drugs, nutrients, and proteins required for these applications.[5,64,65] An increasing number of biologic drugs including recombinant proteins and antibodies are more prone to degradation than other synthetic drugs. Therefore, biologics protection inside hydrogels may lead to increased drug half-life. In addition, the release of drugs and nutrients from the hydrogel to the target site can be controlled by rational hydrogel design.[5] The diffusion of particles inside the hydrogel depends on the mesh size. For particles smaller than the mesh radius, diffusion will be largely controlled by the particle size according to the Stokes−Einstein equation. However, diffusion will be affected to some extent by friction and particle retention, more pronouncedly for small mesh and large particle sizes, thus increasing the release time from the hydrogel network. Hydrogels have been designed to delay drug release by mechanical deformation,[66−68] network degradation,[69,70] and hydrogel swelling.[71,72] In most instances, the three strategies lead to changes in mesh size that modulate diffusion.[5] Understanding the factors that control drug and biologics diffusion in hydrogels is instrumental to designs targeted at biomedical applications such as drug delivery, implants, and regenerative medicine.

It is important to emphasize that particle diffusion in hydrogels is impacted by experimental conditions such as pH, ionic strength,[42] and temperature, as well as potential particle-hydrogel interactions.[27] A study of the effect of pH and ionic strength conducted for different fluorescent dyes showed that the difference between the diffusion coefficients in pure water and agarose gels of the charged fluorescent dye rhodamine decreases with the increase of NaCl concentration from 0.1 mM to 10 mM,[42] likely due to the screening of electrostatic interactions between the hydrogel and the fluorophore. However, the difference in diffusion coefficients is negligible from 10 mM to 100 mM NaCl.[42] A pH effect on rhodamine's diffusion coefficient was also observed: the largest differences between diffusion coefficients in pure water and agarose gels occur from pH 5 to 10.[42] Factors such as pH, ionic strength, and particle-hydrogel interactions are interrelated; for instance, the ionic strength and pH will modulate the partial and net charges of the hydrogels and the diffusing particles, hence influencing electrostatic hydrogel-particle interactions and the diffusion coefficient. Specifically, the effect of pH on the diffusion coefficient will depend on the presence of ionizable groups (and their pK_a values) in the diffusing particle and hydrogel, which will determine the resulting charges and the interactions that will take place.

In addition to the overall charge, other chemical and structural factors have been reported to contribute to molecular diffusion in hydrogels. Specifically, the penetration capability in mucin gels of peptides with different net charges and various hydrophobic amino acid compositions has been determined recently.[27] This study shows that peptides with net positive charge penetrate less than negatively charged peptides in mucin gels due to their anionic nature. However, this work establishes that the net charge does not properly explain the penetration differences observed, identifying that the spatial configuration of charged and hydrophobic groups, as well as specific interactions with the mucin gel significantly impact peptide penetration capabilities.[27]

Temperature is another important factor, as diffusion coefficients increase with temperature following an exponential dependence. The method proposed here should be valid to test the effect of these factors in particle diffusion. For example, the mixtures of hydrogel/fluorescent particle solution can be incubated at different temperatures during the diffusion time to determine the impact of temperature on particle diffusion. In addition, the particle solutions can be prepared at various ionic strengths and pH conditions to test the effect of these factors on diffusion and penetration.

The possibility to tune hydrogel properties such as overall size, shape, mesh size, chemical composition, swelling capability, stiffness, and overall function, broadens the number of hydrogel applications. Thus, methods to determine particle diffusion that adapt to different hydrogel properties and hydrogelation processes are necessary. Among those properties, hydrogel stiffness is an important consideration. For instance, soft hydrogels are currently used for injectable applications,[73] to enhance cell proliferation in tissue engineer-

https://doi.org/10.1021/acsomega.4c06984
ACS Omega 2025, 10, 10852−10865

ing,[73] and as models to study cell response to mechanical forces.[74] A few methods to determine diffusion coefficients use hydrogel slicing to analyze concentration gradient profiles; however, slicing might not be possible for soft hydrogels. These methods typically depend on extracting the diffusing particle and in some instances, the hydrogel is dissolved with harsh solvents.[75] Such procedures may lead to additional experimental errors and will likely compromise the function of delicate biomolecules such as proteins. Organic or harsh solvents typically degrade and unfold proteins, which could impair tests correlating diffusivity and protein function. In addition, the techniques used to monitor particle diffusion play an important role in method implementation. The costs associated with user training and equipment purchase must be considered. Many methods to study diffusion in hydrogels depend on imaging techniques that require the adjustment of the hydrogel shape and size to microfluidic chips or microscope slides.[47,76] However, the hydrogelation process might not be possible in such vessels.

We have described here a simple method to determine particle penetration distances and diffusion coefficients in soft agarose hydrogels. The hydrogels were segmented by careful pipetting with a wide bore tip, as slicing is impractical due to the low stiffness. We have analyzed particle concentration gradients generated by diffusion using fluorescence spectroscopy in a microplate reader. This combination has several advantages: 1) the possibility of multiple, simultaneous measurements depending on the microplate size (96-well microplates were used in this study); 2) the potential to analyze the diffusion of proteins in protein-based hydrogels,[77,78] in contrast to methods using UV absorbance spectroscopy for which the hydrogel can interfere in the measurement; 3) the measurements are done directly in hydrogel sections. Thus it is not necessary to release the diffusing solute or dissolve the hydrogel.

In addition, the method described here does not impose restrictions on hydrogel size. Thus, the hydrogelation reaction does not have to be confined to microfluidic devices, microscope slides, or specific cuvette sizes. This advantage is important for hydrogelation processes requiring constant monitoring, for example when pH gradients drive hydrogelation or swelling.[79] Certain proteins involved in the inflammatory response,[80−82] specifically the inflammasome adaptor protein ASC and its isoforms have a strong tendency to polymerize forming intricate filament networks.[83−87] Recently, we have leveraged this property to form noncovalent hydrogels by pH-driven polymerization of ASC isoforms.[88] The hydrogelation process requires a gradual pH increase and constant monitorization of the pH.[88] Abrupt pH changes will prompt protein precipitation at the expense of hydrogelation. Therefore, forming hydrogels with ASC isoforms in a microfluidic device or small cuvette is challenging. Furthermore, many noncovalent hydrogels tend to be of low stiffness, such as ASC-inspired hydrogels.[88] In such cases, hydrogel sectioning by slicing is not possible. In contrast, our method is suitable for soft hydrogels.

CONCLUSIONS

We have shown the possibility of determining particle penetration distances and diffusion coefficients of fluorescent particles diffusing in soft agarose hydrogels. Our method is based on extracting sections of the hydrogels to analyze particle concentration gradients as a function of penetration distance by measuring fluorescence intensity with a microplate reader. We tested the method's performance in agarose hydrogels of three different percentages with diffusing particles of various chemical compositions and sizes, therefore allowing a broad range of diffusion times.

The agarose percentages were chosen to produce hydrogels of low stiffness which are more suited for injectable and sprayable applications. However, in principle, our method can also be used for stiff hydrogels. Importantly, other methods to study diffusion by sectioning have not been applied to soft hydrogels. Our results with fluorescein, a soluble small aromatic molecule, and the proteins mNeonGreen and BSA, show that the method is convenient for analyzing the diffusion of small drugs and biologics of various sizes in hydrogels with potential applications in drug delivery and tissue engineering. We have shown that the agarose percentage influences the penetration distances of the particles, resulting in deeper penetration at lower percentages. These results can be explained by the pore size analysis of the 0.1% and 0.2% agarose hydrogels, revealing that the former has a slightly larger number of pores in the 26−100 μm^2 range. We have observed more penetration at longer diffusion times and smaller particle sizes, demonstrating that the method can detect differences in penetration distances under various diffusion conditions. This capability is particularly useful for assessing particle-hydrogel interactions, as determining the diffusion coefficients in these circumstances is challenging. Still, relevant information on drug/biologic retention/release can be inferred from the penetration distances.

The diffusion coefficients obtained for the three particles are in very good agreement with previously reported data (Table 1). The D values for fluorescein in agarose and hydroxyethyl cellulose hydrogels are similar and smaller than in water as expected. For mNeonGreen, the D value in agarose is smaller than that of the green fluorescent protein in water, having both proteins comparable sizes, which is also an expected result. The D values of BSA in different agarose percentages vary depending on the pH and ionic strength (Table 1). Lower values of the BSA diffusion coefficient ($0.23-0.34 \times 10^{-4}$ mm^2/s) were found at high ionic strength (0.1 M NaCl)[63] in accord with the values obtained here ($0.34-0.39 \times 10^{-4}$ mm^2/s) also using 0.1 M NaCl. Overall, the good agreement between the reported and obtained diffusion coefficients demonstrates the validity of the method.

In conclusion, the main advantages of the method developed within this work are its simplicity and adaptability. The overall procedure does not require extensive user training or maneuvering complex equipment, thus leading to lower cost and higher time effectiveness. Importantly, the method can be adapted to hydrogels of various compositions, shapes, and sizes, as well as different hydrogelation processes. The technique presented here responds to solutes of different chemical natures and sizes, broadening its applications. Finally, we have shown the sensitivity of the method to variations in the diffusion conditions. This property can be leveraged to study hydrogel−solute interactions in designs for controlled release by identifying differences in penetration distances.

METHODS

A. Chemicals. High melting agarose (TopVision Agarose with high melting and gelling temperature), Dylight488 NHS ester (Dylight 488), and fluorescein disodium salt were purchased from Thermo Scientific. Bovine serum albumin

https://doi.org/10.1021/acsomega.4c06984
ACS Omega 2025, 10, 10852−10865

(BSA) was purchased from Sigma. Sodium chloride (NaCl), Tris(hydroxymethyl)aminomethane (Tris), sodium phosphate monobasic anhydrous (NaH_2PO_4), and dimethyl sulfoxide (DMSO) were purchased from Fisher.

B. Solutions of Fluorescent Particles. The fluorophores used were fluorescein, the intrinsically fluorescent protein mNeonGreen, and Dylight 488 NHS ester, with the following excitation and emission wavelengths: 498 and 517 nm (fluorescein), 506 and 517 nm (mNeonGreen), and 493 and 518 nm (Dylight 488 NHS ester), respectively.

Preparation of Fluorescein Solutions. A concentration of 0.1 mM fluorescein with an average molecular weight of 0.3 kDa was prepared using 20 mM sodium phosphate buffer at pH 7.8. The absorbance of the dissolved fluorescein was measured with a UV−vis spectrophotometer, and the concentration was determined using the Beer−Lambert law. The solution was subjected to serial dilution to achieve 20, 40, 60, 80, 100, 120, 140, 160, 180, and 200 nM. These concentrations were used to generate the calibration plot for the fluorescein diffusion experiment. All fluorescein stocks and solutions were prepared fresh for each experiment.

Labeling of Bovine Serum Albumin with Dylight 488 NHS Ester and Solution Preparation. A 0.15 mM solution of BSA (average molecular weight of 66.4 kDa) was labeled with Dylight 488 NHS ester (average molecular weight of 753.04 Da) by dissolving 10 mg of BSA in 1 mL of labeling buffer containing 20 mM of anhydrous NaH_2PO_4 at pH 7.4 and 100 mM NaCl. Next, 0.4 mg of Dylight 488 was dissolved in 50 μL of DMSO and added dropwise to 950 μL of the labeling buffer. This solution was gently incorporated into 1 mL of 0.15 mM BSA and the mixture was incubated at room temperature for 1 h in a tube rotator operating at 50 rpm. The labeled BSA was purified using 2 consecutive disposable PD10 desalting columns. The final molar ratio of BSA to Dylight 488 was 1:2.6. The purity of the labeled material was determined by mass spectrometry. The concentration was determined using absorbance spectroscopy at the recommended BSA and Dylight 488 wavelengths of 280 and 493 nm, respectively, obtained from a UV−vis spectrophotometer. The degree of labeling was determined by mass spectrometry as indicated below. The solution of Dylight-labeled BSA was diluted with the labeling buffer to achieve 2, 4, 6, 8, 10, 12, 14, 16, 18, and 20 μM solutions used to obtain the standard curve for the experiment.

Expression and Purification of mNeonGreen and Solution Preparation. To overexpress mNeonGreen, we used the plasmid pDream2.1 carrying the gene encoding for the protein. This plasmid, a gift from Prof. Muñoz (UC Merced), was transformed into *Escherichia coli* BL21(DE3) cells. The transformed bacteria were grown in Luria−Bertani broth overnight and the culture was diluted the next morning with fresh media before induction. Protein expression was induced with 1 mM isopropyl β-D-thiogalactopyranoside (IPTG) at 37 °C for 4 h once the bacteria reached an optical density at 280 nm (OD_{280}) of 0.7−1. Subsequently, cells were harvested by centrifugation at 8,000 rpm for 30 min and resuspended by stirring at 4 °C in 20 mM Tris (pH 8.0), 20 mM imidazole, 500 mM NaCl, and phenylmethylsulfonyl fluoride (PMSF) as a protease inhibitor. Cells were lysed by sonication at 20 kHz for 48 min on ice with on−off cycles of 15 and 45 s, respectively. The lysate was subjected to ultracentrifugation at 35,000 rpm for 30 min at 4 °C. The supernatant was filtered with a 0.45 μm pore filter and stored at −80 °C.

The N-terminal six-histidine tag in mNeonGreen allowed protein purification by nickel affinity chromatography with an elution gradient of imidazole from 20 to 500 mM in an HPLC using a flow rate of 1 mL/min. The protein was dialyzed in 20 mM Tris at pH 8.0 and stock solutions were prepared at concentrations determined by UV−vis spectroscopy. The protein concentrations used to generate the standard plot were 20, 40, 60, 80, 100, 120, and 148 μM, achieved by diluting the stock solutions with 20 mM Tris buffer at pH 8.0. We tested the stability of mNeonGreen solutions by monitoring the intensity of fluorescence emission in the absence of hydrogel daily for 5 days. The intensity did not show a downward trend and remained constant within the error of the measurements.

For each diffusion experiment, three independent calibration sets were prepared for each fluorescent particle (fluorescein, mNeonGreen, and BSA) at the concentrations indicated above. The largest concentration is considered the reference value (C_0).

C. Preparation of Agarose Hydrogels. The different percentages of agarose hydrogels (0.05%, 0.1%, and 0.2%) were prepared by mixing 0.05, 0.1, and 0.2 g of agarose in 100 mL of Milli-Q water, respectively. The agarose was dissolved by heating the mixture at a temperature of 101 °C for 150 s using a microwave. The solutions were let to cool for 10 min. A volume of 1.5 mL of the resulting solutions was transferred to 2 mL microcentrifuge cylindrical tubes for overnight hydrogelation at room temperature. We checked positive hydrogel formation by observing significantly reduced flowability when inverting the Eppendorf tubes.

We prepared two (mNeonGreen) and three (fluorescein and BSA) independent hydrogels for each diffusion experiment at the three different agarose percentages and diffusion times.

D. Diffusion Experiments, Hydrogel Sectioning, and Section Homogenization. Solutions (200 μL) of the fluorescent particles at the initial concentrations (C_0: 200 nM fluorescein, 20 μM Dylight 488-BSA, and 148 μM mNeonGreen) were added to 1.5 mL of the different agarose hydrogels. This step was considered the initial time point ($t = 0$) for the diffusion of the particles. The volume of the hydrogels increased from 1.5 to 1.7 mL in less than 4 h due to swelling. Potential swelling effects on diffusion were disregarded based on the small increase in the total hydrogel volume. Diffusion times were 4, 14, and 24 h for fluorescein; 6, 14, 24, 48 h, and 5 days for mNeonGreen; and 48 h and 5 days for Dylight 488-BSA. The diffusion times required for the experiments depend on particle size.

Once the diffusion experiments finished, the hydrogel sections were extracted every 3 mm (approximately 200 μL) along the normal to the hydrogel's top surface with a wide bore micropipette. For the discretization experiments, sections were extracted every 4 mm (approximately 270 μL). The bottom of the Eppendorf tube has a different shape that could affect diffusion. Thus, a hydrogel volume of 0.1 mL at the tube's base was not used for measurements.

The extracted hydrogel sections were homogenized for subsequent fluorescence intensity measurements. Homogenization was performed by pipetting for 5 s. The consistency of the 0.05% and 0.1% agarose hydrogel sections was liquid-like and did not display notable differences before and after homogenization. In contrast, the consistency of the 0.2% agarose hydrogel sections became more liquid after homogenization and analogous to the 0.05 and 0.1% agarose hydrogel

https://doi.org/10.1021/acsomega.4c06984
ACS Omega 2025, 10, 10852−10865

sections. We tested the potential effects of homogenization time and method on fluorescence intensity and concentration values. For this purpose, we performed 4 h fluorescein diffusion experiments in 0.05%, 0.1%, and 0.2% agarose hydrogels and homogenized hydrogel sections by pipetting for 5 s, 15 s, and low-speed (3 rpm) vortexing for 15 s. No significant differences were observed in fluorescence intensity or concentration values (Figure S1). Thus, we concluded that vortexing or pipetting for 5 s is sufficient for thorough homogenization.

Laboratory work involving fluorophores was done in dark rooms with dimmed light sources. All diffusion experiments at each agarose percentage and diffusion time were performed in two (mNeonGreen) and three (fluorescein and BSA) independently prepared hydrogels.

E. Fluorescence Emission and Particle Concentration Measurements at Different Penetration Distances in Agarose Hydrogels. Volumes of 100 μL from the 200 μL homogenized hydrogel sections were added to a 96-round well flat-bottom black microplate. By extracting a hydrogel volume larger than the one required in the microplate well, we ensure that all sections have the same volume, thus avoiding errors in concentration measurements. In addition, 100 μL of the corresponding standard solutions are added to the same microplate. The fluorescence emission spectra and emission intensities at specific wavelengths were obtained with the spectral scan and end point functions of a microplate reader CLARIOstar Plus from BMG Labtech.

Two (mNeoGreen) and three (fluorescein and BSA) fluorescence intensity values were obtained for each extracted hydrogel section, corresponding to the independently prepared hydrogels. The fluorescence intensity values were background corrected using the pertinent buffer solutions. Three standard solutions of fluorescein, mNeonGreen, and BSA were prepared independently to obtain independent fluorescence intensity measurements at each concentration value. The resulting values were background corrected using the corresponding buffer solutions and averaged to obtain the calibration plot correlating fluorescence intensity to particle concentration (Figure S2).

The calibration plots were used to determine independent concentration values (C_i) at each penetration distance based on the fluorescence intensity of the corresponding hydrogel section. We determined average and standard deviation values of the concentration ratios (C_i/C_0) using the independent C_i values (2 for mNeonGrenn and three for fluorescein and BSA) and the initial concentrations measured as indicated above. The calibration plot for mNeonGreen showed a plateau at high protein concentrations, likely due to protein aggregation interfering with fluorescence emission. Thus, the data were linearized to extrapolate the C_i values to reduce errors.

The parameters for acquiring spectral scans for fluorescein matched the recommended excitation wavelength of 483 ± 14 nm (476−490 nm) and the emission spectra were acquired from 500 to 600 nm with a step width of 2 nm. The highest concentration of fluorophore in the black 96-well plate and the recommended maximum emission wavelength were selected for gain adjustment. The emission wavelength corresponding to the maximum intensity was used for the end point scan function of the microplate reader. The enhanced dynamic range option was selected for the end point scan because it allows for gain adjustment based on the highest intensity/concentration. The overall intensity value obtained from the microplate reader can be increased or decreased by modifying the gain value. This process was repeated for mNeonGreen (excitation of 480 ± 10 nm, emission range of 500 to 600 nm), and Dylight 488-BSA (excitation of 487 ± 16 nm, emission range of 500 to 600 nm).

F. Detection Limits and Working Concentration Ranges. The specified detection limit for fluorescence intensity measurements in the microplate reader CLARIOstar Plus from BMG Labtech is 0.35 pM using black bottom microplates (detection from the top). The minimum required concentrations of the fluorescent particles will depend on the quantum yields and extinction coefficients of the fluorophores. Typical particle concentrations for fluorescence intensity experiments range from nanomolar to micromolar. The concentrations used in this work do not represent the minimum values required and were chosen to provide large values of fluorescence emission in the bottom sections of the hydrogels to decrease potential errors. Additional experiments are required to determine the minimum concentration values and associated measurement errors. The minimum hydrogel volume required is 1.5 mL for the experimental setup indicated, i.e., hydrogelation in 2 mL microcentrifuge cylindrical tubes, extraction of hydrogel sections every 3 mm (~200 μL), and acquisition of 8 penetration distance points for the concentration profile.

G. Mass Spectrometry of Dylight 488-BSA. A purified Dylight 488-BSA sample at 22.6 μM was analyzed using an electrospray ionization mass spectrometer (Q-Exactive Hybrid Quadrupole-Orbitrap, Thermo) coupled to a UHPLC system (Vanquish, Thermo). A volume of 10 μL was injected into a reverse-phase column (Acclaim 200 C18, 2.6 μm, Thermo) at a flow rate of 300 μL/min. Mass spectra were recorded with a mass range of 10 kDa to 160 kDa. The resulting spectra representing signal intensity versus mass-to-charge ratio were analyzed using BioPharma 2.0 software (Thermo).

The mass spectrometry results (Figure S3) indicate the following percentages of Dylight 488 labeled-BSA species: 48.6% and 47.8%, with 3:1 and 2:1 fluorophore to protein ratio, respectively, and 3.6% of a species with two Dylight 488 moieties, but only one covalently attached.

H. Sample Preparation for Scanning Electron Microscopy (SEM). Volumes of 50 μL of agarose hydrogels at different percentages were flash-frozen in liquid nitrogen followed by lyophilization. The samples were mounted on a double-sided conductive carbon adhesive tape with one side attached to the SEM aluminum specimen mount. The samples were coated for 1 min with a sputter coater at a vacuum of 0.07 Torr leading to a gold film of approximately 10 nm thick. Images were obtained with a Zeiss Gemini 500 Field Emission Scanning Electron Microscope operating at a voltage of 3 kV by using either in-lens or secondary electron detectors. The Fiji open-source software was used for analysis. The images designated for analysis were selected, and the original scale bar of each image was entered to determine the distance that would be used for analysis. The following Fiji options were used: "duplicate" to protect the original image, "edit" to invert the image, "analyze particles" and "measure" to determine hydrogel pore dimensions.

I. Details on the Fitting of the Experimental Data. The diffusion coefficient of each fluorescent particle was obtained by fitting the experimental data into a 1-dimensional diffusion model (eq 1) using the QtGrace software.

eq 1 was transformed into eq 2 by assuming $m = 1$.

https://doi.org/10.1021/acsomega.4c06984
ACS Omega 2025, 10, 10852−10865

$$y = B_1\cos(\pi x/L)e^{-\pi^2 Dt/L^2} + C_f \quad (2)$$

where: $y = \frac{C_i}{C_0}$, B_1, D, *and* C_f, already defined for eq 1, were obtained by nonlinear regression. L = 24 mm, C_f was estimated based on the volume considered for diffusion (1.6 mL), and t is the diffusion time (24 h for fluorescein and 5 days for mNeonGreen and Dylight 488-BSA). Initial guesses for the three unknowns (B_m, D, *and* C_f) for fluorescein were 0.6161, 0.0001 (boundaries 0−0.9), and 0.125, respectively; mNeonGreen, 0.25 (boundaries 0−0.6162), 0.0001 (boundaries 0−1), and 0.125, Dylight 488-BSA 0.25, 0.0001 (boundaries from 0−1), and 0.125. The average and standard deviation values of the diffusion coefficient of each fluorescent particle were obtained from two to three independent diffusion experiments. Data on the goodness of fit are shown in Table S1.

J. Limitations and Constraints.

Hydrogel.

1. The hydrogel dimensions are constrained by the minimum volume required in the wells of the microplate for proper detection of the fluorescence intensity depending on the adjustment of the microplate reader's focal height.
2. The method is not applicable to hydrogels that need to be formed in microfluidic devices due to constraints in dimensions.
3. The level of discretization of the hydrogel is determined by its volume and dimensions, as well as the minimum number of data points required to properly represent the concentration gradient profile.
4. Soft hydrogels can be sectioned by aspiring with micropipettes attached to wide bore tips. Sectioning with micropipettes leads to good control of the hydrogel volume, hence reducing errors in concentration measurements. Stiff hydrogels need to be sliced and placed on the wells of the microplate reader. Measurements of hydrogel volume are less accurate and precise.

Fluorescent Particles.

1. Most fluorophores are sensitive to light: laboratory work with fluorescent particles often needs to be performed in dark rooms, which may lead to a potential increase in errors, specifically pertaining to hydrogel sectioning.
2. The intensity of fluorescence emission strongly depends on the type of fluorophore used due to differences in quantum yields and extinction coefficients, hence impacting the required fluorophore concentration.
3. Nonfluorescent particles need to be chemically modified by adding a fluorescent moiety. In such cases, chemical reactions and purification processes are required. Laboratory assays and techniques for molecular characterization, like mass spectrometry, might be needed to determine the labeling efficiency and the incorporation of the fluorophore.

Particle Size.

1. The large dimensions of the hydrogels may require long experimental times to track the diffusion of large particles, such as proteins, in different hydrogel sections. The protein stability may be compromised if the diffusion experiment is performed at ambient temperature. Smaller hydrogel volumes and hydrogels with larger pore sizes could reduce experimental time.

Diffusion Coefficient Determination.

1. The method herein described assumes Fickian diffusion to determine the diffusion coefficients based on the analysis of particle concentration profiles as a function of diffusion distance.[55] For instance, the presence of strong hydrogel-particle interactions and the modification of the hydrogel structure during diffusion could lead to non-Fickian behavior.
2. The method is valid for determining the penetration distances of particles in hydrogels.

■ ASSOCIATED CONTENT

Supporting Information

The Supporting Information is available free of charge at https://pubs.acs.org/doi/10.1021/acsomega.4c06984.

Fluorescence intensity data of differently homogenized hydrogel sections, calibration plots of fluorescein, mNeonGreen, fluorescent BSA, mass spectrometry data of fluorescent BSA, and goodness of the fitting of the experimental data to the 1D diffusion model (PDF)

■ AUTHOR INFORMATION

Corresponding Author

Eva de Alba − *Department of Bioengineering, University of California, Merced, California 95343, United States;* orcid.org/0000-0002-4794-5728; Email: edealbabastarrechea@ucmerced.edu

Author

Ayomide J. Adeoye − *Department of Bioengineering, University of California, Merced, California 95343, United States*

Complete contact information is available at: https://pubs.acs.org/10.1021/acsomega.4c06984

Notes

The authors declare no competing financial interest.

■ ACKNOWLEDGMENTS

A.J.A. and E.d.A. acknowledge the National Institute of Allergy and Infectious Diseases of the National Institutes of Health for financial support under award number R21AI178831 (to E.d.A.) and support from the NSF-CREST Center for Cellular and Biomolecular Machines at the University of California, Merced (NSF-HRD-2112675). We thank the UC Merced Imaging facility for access to the SEM equipment. We are grateful to Mourad Sadqi for mass spectrometry data acquisition and analysis. We thank Suzanne Sandin for the mNeonGreen samples. The content of this publication is solely the responsibility of the authors and does not necessarily represent the official views of the National Institutes of Health or the National Science Foundation.

■ REFERENCES

(1) Majcher, M. J.; Hoare, T. Applications of Hydrogels. *Funct. Biopolym.* **2019**, 453.

(2) Ullah, F.; Othman, M. B. H.; Javed, F.; Ahmad, Z.; Akil, H. M. Classification, Processing and Application of Hydrogels: A Review. *Mater. Sci. Eng. C* **2015**, *57*, 414.

(3) Sánchez-Cid, P.; Jiménez-Rosado, M.; Romero, A.; Pérez-Puyana, V. Novel Trends in Hydrogel Development for Biomedical Applications: A Review. *Polymers* **2022**, *14*, 3023.
(4) Correa, S.; Grosskopf, A. K.; Lopez Hernandez, H.; Chan, D.; Yu, A. C.; Stapleton, L. M.; Appel, E. A. Translational Applications of Hydrogels. *Chem. Rev.* **2021**, *121*, 11385.
(5) Li, J.; Mooney, D. J. Designing Hydrogels for Controlled Drug Delivery. *Nat. Rev. Mater.* **2016**, *1*, 16071.
(6) Bernhard, S.; Tibbitt, M. W. Supramolecular Engineering of Hydrogels for Drug Delivery. *Adv. Drug Delivery Rev.* **2021**, *171*, 240.
(7) Nottelet, B.; Buwalda, S.; van Nostrum, C. F.; Zhao, X.; Deng, C.; Zhong, Z.; Cheah, E.; Svirskis, D.; Trayford, C.; van Rijt, S.; Ménard-Moyon, C.; Kumar, R.; Kehr, N. S.; de Barros, N. R.; Khademhosseini, A.; Kim, H. J.; Vermonden, T. Roadmap on Multifunctional Materials for Drug Delivery. *J. Phys. Mater.* **2024**, *7*, No. 012502.
(8) Vázquez-González, M.; Willner, I. Stimuli-Responsive Biomolecule-Based Hydrogels and Their Applications. *Angew. Chem. - Int. Ed.* **2020**, *59*, 15342.
(9) Chen, J.; Peng, Q.; Peng, X.; Han, L.; Wang, X.; Wang, J.; Zeng, H. Recent Advances in Mechano-Responsive Hydrogels for Biomedical Applications. *ACS Appl. Polym. Mater.* **2020**, *2*, 1092.
(10) Neumann, M.; di Marco, G.; Iudin, D.; Viola, M.; van Nostrum, C. F.; van Ravensteijn, B. G. P.; Vermonden, T. Stimuli-Responsive Hydrogels: The Dynamic Smart Biomaterials of Tomorrow. *Macromolecules* **2023**, *56*, 8377.
(11) O'Neill, H. S.; Herron, C. C.; Hastings, C. L.; Deckers, R.; Lopez Noriega, A.; Kelly, H. M.; Hennink, W. E.; McDonnell, C. O.; O'Brien, F. J.; Ruiz-Hernández, E.; Duffy, G. P. A Stimuli Responsive Liposome Loaded Hydrogel Provides Flexible On-Demand Release of Therapeutic Agents. *Acta Biomater.* **2017**, *48*, 110.
(12) Yanev, P.; van Tilborg, G. A. F.; Boere, K. W. M.; Stowe, A. M.; van der Toorn, A.; Viergever, M. A.; Hennink, W. E.; Vermonden, T.; Dijkhuizen, R. M. Thermosensitive Biodegradable Hydrogels for Local and Controlled Cerebral Delivery of Proteins: MRI-Based Monitoring of In Vitro and In Vivo Protein Release. *ACS Biomater. Sci. Eng.* **2023**, *9* (2), 760.
(13) Pandit, A. H.; Nisar, S.; Imtiyaz, K.; Nadeem, M.; Mazumdar, N.; Rizvi, M. M. A.; Ahmad, S. Injectable, Self-Healing, and Biocompatible N,O-Carboxymethyl Chitosan/Multialdehyde Guar Gum Hydrogels for Sustained Anticancer Drug Delivery. *Biomacromolecules* **2021**, *22* (9), 3731.
(14) Chen, J.; Luo, J.; Feng, J.; Wang, Y.; Lv, H.; Zhou, Y. Spatiotemporal controlled released hydrogels for multi-system regulated bone regeneration. *J. Controlled Release* **2024**, *372*, 846–861.
(15) Van Vlierberghe, S.; Dubruel, P.; Schacht, E. Biopolymer-Based Hydrogels As Scaffolds for Tissue Engineering Applications: A Review. *Biomacromolecules* **2011**, *12* (5), 1387–1408.
(16) Mantha, S.; Pillai, S.; Khayambashi, P.; Upadhyay, A.; Zhang, Y.; Tao, O.; Pham, H. M.; Tran, S. D. Smart Hydrogels in Tissue Engineering and Regenerative Medicine. *Materials* **2019**, *12*, 3323.
(17) Xu, F.; Dawson, C.; Lamb, M.; Mueller, E.; Stefanek, E.; Akbari, M.; Hoare, T. Hydrogels for Tissue Engineering: Addressing Key Design Needs Toward Clinical Translation. *Front. Bioeng. Biotechnol.* **2022**, *10*, No. 849831.
(18) Zhu, J.; Marchant, R. E. Design Properties of Hydrogel Tissue-Engineering Scaffolds. *Expert Rev. Med. Devices* **2011**, *8*, 607.
(19) Davari, N.; Bakhtiary, N.; Khajehmohammadi, M.; Sarkari, S.; Tolabi, H.; Ghorbani, F.; Ghalandari, B. Protein-Based Hydrogels: Promising Materials for Tissue Engineering. *Polymers* **2022**, *14*, 986.
(20) Zhao, Y.; Song, S.; Ren, X.; Zhang, J.; Lin, Q.; Zhao, Y. Supramolecular Adhesive Hydrogels for Tissue Engineering Applications. *Chem. Rev.* **2022**, *122*, 5604.
(21) Tindell, R. K.; McPhail, M. J.; Myers, C. E.; Neubauer, J.; Hintze, J. M.; Lott, D. G.; Holloway, J. L. Trilayered Hydrogel Scaffold for Vocal Fold Tissue Engineering. *Biomacromolecules* **2022**, *23* (11), 4469.
(22) Sandin, S. I.; Gravano, D. M.; Randolph, C. J.; Sharma, M.; de Alba, E. Engineering of Saposin C Protein Chimeras for Enhanced Cytotoxicity and Optimized Liposome Binding Capability. *Pharmaceutics* **2021**, *13* (4), 583.
(23) Axpe, E.; Chan, D.; Offeddu, G. S.; Chang, Y.; Merida, D.; Hernandez, H. L.; Appel, E. A. A Multiscale Model for Solute Diffusion in Hydrogels. *Macromolecules* **2019**, *52* (18), 6889–6897.
(24) Cukier, R. I. Diffusion of Brownian Spheres in Semidilute Polymer Solutions. *Macromolecules* **1984**, *17* (2), 252–255.
(25) Fujiyabu, T.; Li, X.; Chung, U.; Sakai, T. Diffusion Behavior of Water Molecules in Hydrogels with Controlled Network Structure. *Macromolecules* **2019**, *52* (5), 1923–1929.
(26) Cohen, M. H.; Turnbull, D. Molecular Transport in Liquids and Glasses. *J. Chem. Phys.* **1959**, *31* (5), 1164–1169.
(27) Samad, T.; Witten, J.; Grodzinsky, A. J.; Ribbeck, K. Spatial Configuration of Charge and Hydrophobicity Tune Particle Transport through Mucus. *Biophys. J.* **2022**, *121* (2), 277–287.
(28) Abune, L.; Wang, Y. Affinity Hydrogels for Protein Delivery. *Trends Pharmacol. Sci.* **2021**, *42* (4), 300–312.
(29) Veith, S. R.; Hughes, E.; Pratsinis, S. E. Restricted Diffusion and Release of Aroma Molecules from Sol-Gel-Made Porous Silica Particles. *J. Controlled Release* **2004**, *99* (2), 315–327.
(30) Masaro, L.; Zhu, X. X. Self-Diffusion of End-Capped Oligo(Ethylene Glycol)s in Poly(Vinyl Alcohol) Aqueous Solutions and Gels. *Macromolecules* **1999**, *32* (16), 5383–5390.
(31) Hajatdoost, S.; Sammon, C.; Yarwood, J. FTIR–ATR Studies of Diffusion and Perturbation of Water in Polyelectrolyte Thin Films. Part 4. Diffusion, Perturbation and Swelling Processes for Ionic Solutions in SPEES/PES Membranes. *Polymer* **2002**, *43* (6), 1821–1827.
(32) Liang, S.; Xu, J.; Weng, L.; Dai, H.; Zhang, X.; Zhang, L. Protein Diffusion in Agarose Hydrogel in Situ Measured by Improved Refractive Index Method. *J. Controlled Release* **2006**, *115* (2), 189–196.
(33) Kosar, T. F.; Phillips, R. J. Measurement of Protein Diffusion in Dextran Solutions by Holographic Interferometry. *AIChE J.* **1995**, *41* (3), 701–711.
(34) McCain, K. S.; Harris, J. M. Total Internal Reflection Fluorescence-Correlation Spectroscopy Study of Molecular Transport in Thin Sol–Gel Films. *Anal. Chem.* **2003**, *75* (14), 3616–3624.
(35) Swaminathan, R.; Hoang, C. P.; Verkman, A. S. Photobleaching Recovery and Anisotropy Decay of Green Fluorescent Protein GFP-S65T in Solution and Cells: Cytoplasmic Viscosity Probed by Green Fluorescent Protein Translational and Rotational Diffusion. *Biophys. J.* **1997**, *72* (4), 1900–1907.
(36) Jiang, F.; Xu, X. W.; Chen, F. Q.; Weng, H. F.; Chen, J.; Ru, Y.; Xiao, Q.; Xiao, A. F. Extraction, Modification and Biomedical Application of Agarose Hydrogels: A Review. *Mar. Drugs* **2023**, *21*, 299.
(37) Lahaye, M. Developments on Gelling Algal Galactans, Their Structure and Physico-Chemistry. *J. Appl. Phycol.* **2001**, *13* (2), 173.
(38) Crespo-Cuevas, V.; Ferguson, V. L.; Vernerey, F. Poroviscoelasto-Plasticity of Agarose-Based Hydrogels. *Soft Matter* **2023**, *19* (4), 790.
(39) Salati, M. A.; Khazai, J.; Tahmuri, A. M.; Samadi, A.; Taghizadeh, A.; Taghizadeh, M.; Zarrintaj, P.; Ramsey, J. D.; Habibzadeh, S.; Seidi, F.; Saeb, M. R.; Mozafari, M. Agarose-Based Biomaterials: Opportunities and Challenges in Cartilage Tissue Engineering. *Polymers* **2020**, *12*, 1150.
(40) Lee, P. Y.; Costumbrado, J.; Hsu, C. Y.; Kim, Y. H. Agarose Gel Electrophoresis for the Separation of DNA Fragments. *J. Visualized Exp.* **2012**, 62.
(41) Khodadadi Yazdi, M.; Taghizadeh, A.; Taghizadeh, M.; Stadler, F. J.; Farokhi, M.; Mottaghitalab, F.; Zarrintaj, P.; Ramsey, J. D.; Seidi, F.; Saeb, M. R.; Mozafari, M. Agarose-Based Biomaterials for Advanced Drug Delivery. *J. Controlled Release* **2020**, *326*, 523.
(42) Fatin-Rouge, N.; Milon, A.; Buffle, J.; Goulet, R. R.; Tessier, A. Diffusion and Partitioning of Solutes in Agarose Hydrogels: The

https://doi.org/10.1021/acsomega.4c06984
ACS Omega 2025, 10, 10852–10865

Relative Influence of Electrostatic and Specific Interactions. *J. Phys. Chem. B* **2003**, *107* (44), 12126.
(43) Stokols, S.; Sakamoto, J.; Breckon, C.; Holt, T.; Weiss, J.; Tuszynski, M. H. Templated Agarose Scaffolds Support Linear Axonal Regeneration. *Tissue Eng.* **2006**, *12* (10), 2777.
(44) Sánchez-Salcedo, S.; Nieto, A.; Vallet-Regí, M. Hydroxyapatite/β-Tricalcium Phosphate/Agarose Macroporous Scaffolds for Bone Tissue Engineering. *Chem. Eng. J.* **2008**, *137* (1), 62.
(45) Miguel, S. P.; Ribeiro, M. P.; Brancal, H.; Coutinho, P.; Correia, I. J. Thermoresponsive Chitosan-Agarose Hydrogel for Skin Regeneration. *Carbohydr. Polym.* **2014**, *111*, 366.
(46) Gong, W.; Wang, R.; Huang, H.; Hou, Y.; Wang, X.; He, W.; Gong, X.; Hu, J. Construction of Double Network Hydrogels Using Agarose and Gallic Acid with Antibacterial and Anti-Inflammatory Properties for Wound Healing. *Int. J. Biol. Macromol.* **2023**, *227*, 698.
(47) Wenger, L.; Hubbuch, J. Investigation of Lysozyme Diffusion in Agarose Hydrogels Employing a Microfluidics-Based UV Imaging Approach. *Front. Bioeng. Biotechnol.* **2022**, *10*, 10.
(48) Westrin, B. A.; Axelsson, A.; Zacchi, G. Diffusion Measurement in Gels. *J. Controlled Release* **1994**, *30* (3), 189−199.
(49) Upadrashta, S. M.; Häglund, B. O.; Sundelöf, L.-O. Diffusion and Concentration Profiles of Drugs in Gels. *J. Pharm. Sci.* **1993**, *82* (11), 1094−1098.
(50) Colombo, I.; Grassi, M.; Lapasin, R.; Pricl, S. Determination of the Drug Diffusion Coefficient in Swollen Hydrogel Polymeric Matrices by Means of the Inverse Sectioning Method. *J. Controlled Release* **1997**, *47* (3), 305−314.
(51) Ge, M.; Sun, J.; Chen, M.; Tian, J.; Yin, H.; Yin, J. A Hyaluronic Acid Fluorescent Hydrogel Based on Fluorescence Resonance Energy Transfer for Sensitive Detection of Hyaluronidase. *Anal. Bioanal. Chem.* **2020**, *412* (8), 1915.
(52) Fakhouri, A. S.; Leight, J. L. Measuring Global Cellular Matrix Metalloproteinase and Metabolic Activity in 3D Hydrogels. *J. Visualized Exp.* **2019**, *2019* (143), No. e59123.
(53) Narayanan, J.; Xiong, J. Y.; Liu, X. Y. Determination of Agarose Gel Pore Size: Absorbance Measurements Vis a Vis Other Techniques. *J. Phys. Conf. Ser.* **2006**, *28* (1), 83.
(54) Kopač, T.; Ručigaj, A.; Krajnc, M. The Mutual Effect of the Crosslinker and Biopolymer Concentration on the Desired Hydrogel Properties. *Int. J. Biol. Macromol.* **2020**, *159*, 557.
(55) Crank, J. *The Mathematics of Diffusion.*, 2nd ed.; Oxford University Press: London, 1975.
(56) Hamada, M.; de Anna, P. A Method to Measure the Diffusion Coefficient in Liquids. *Transp Porous Media* **2023**, *146* (1), 463−474.
(57) Richbourg, N. R.; Peppas, N. A. High-Throughput FRAP Analysis of Solute Diffusion in Hydrogels. *Macromolecules* **2021**, *54* (22), 10477.
(58) Geonnotti, A. R.; Furlow, M. J.; Wu, T.; DeSoto, M. G.; Henderson, M. H.; Kiser, P. F.; Katz, D. F. Measuring Macrodiffusion Coefficients in Microbicide Hydrogels via Postphotoactivation Scanning. *Biomacromolecules* **2008**, *9* (2), 748.
(59) Liarzi, O.; Epel, B. L. Development of a Quantitative Tool for Measuring Changes in the Coefficient of Conductivity of Plasmodesmata Induced by Developmental, Biotic, and Abiotic Signals. *Protoplasma* **2005**, *225* (1−2), 67.
(60) Potma, E. O.; De Boeij, W. P.; Bosgraaf, L.; Roelofs, J.; Van Haastert, P. J. M.; Wiersma, D. A. Reduced Protein Diffusion Rate by Cytoskeleton in Vegetative and Polarized Dictyostelium Cells. *Biophys. J.* **2001**, *81* (4), 2010.
(61) Yohannes, G.; Wiedmer, S. K.; Elomaa, M.; Jussila, M.; Aseyev, V.; Riekkola, M. L. Thermal Aggregation of Bovine Serum Albumin Studied by Asymmetrical Flow Field-Flow Fractionation. *Anal. Chim. Acta* **2010**, *675* (2), 191.
(62) Karlsson, D.; Zacchi, G.; Axelsson, A. Electronic Speckle Pattern Interferometry: A Tool for Determining Diffusion and Partition Coefficients for Proteins in Gels. *Biotechnol. Prog.* **2002**, *18* (6), 1423.
(63) Gutenwik, J.; Nilsson, B.; Axelsson, A. Determination of Protein Diffusion Coefficients in Agarose Gel with a Diffusion Cell. *Biochem Eng. J.* **2004**, *19* (1), 1.
(64) Meis, C. M.; Salzman, E. E.; Maikawa, C. L.; Smith, A. A. A.; Mann, J. L.; Grosskopf, A. K.; Appel, E. A. Self-Assembled, Dilution-Responsive Hydrogels for Enhanced Thermal Stability of Insulin Biopharmaceuticals. *ACS Biomater. Sci. Eng.* **2021**, *7* (9), 4221.
(65) Osorno, L. L.; Brandley, A. N.; Maldonado, D. E.; Yiantsos, A.; Mosley, R. J.; Byrne, M. E. Review of Contemporary Self-Assembled Systems for the Controlled Delivery of Therapeutics in Medicine. *Nanomaterials* **2021**, *11*, 278.
(66) Liu, T. Y.; Hu, S. H.; Liu, T. Y.; Liu, D. M.; Chen, S. Y. Magnetic-Sensitive Behavior of Intelligent Ferrogels for Controlled Release of Drug. *Langmuir* **2006**, *22* (14), 5974.
(67) Zhao, X.; Kim, J.; Cezar, C. A.; Huebsch, N.; Lee, K.; Bouhadir, K.; Mooney, D. J. Active Scaffolds for On-Demand Drug and Cell Delivery. *Proc. Natl. Acad. Sci. U. S. A.* **2011**, *108* (1), 67.
(68) Mitragotri, S.; Blankschtein, D.; Langer, R. Ultrasound-Mediated Transdermal Protein Delivery. *Science* **1995**, *269* (5225), 850.
(69) Boontheekul, T.; Kong, H. J.; Mooney, D. J. Controlling Alginate Gel Degradation Utilizing Partial Oxidation and Bimodal Molecular Weight Distribution. *Biomaterials* **2005**, *26* (15), 2455.
(70) Ishihara, M.; Obara, K.; Ishizuka, T.; Fujita, M.; Sato, M.; Masuoka, K.; Saito, Y.; Yura, H.; Matsui, T.; Hattori, H.; Kikuchi, M.; Kurita, A. Controlled Release of Fibroblast Growth Factors and Heparin from Photocrosslinked Chitosan Hydrogels and Subsequent Effect on in Vivo Vascularization. *J. Biomed. Mater. Res., Part A* **2003**, *64A* (3), 551.
(71) Mumper, R. J.; Huffman, A. S.; Puolakkainen, P. A.; Bouchard, L. S.; Gombotz, W. R. Calcium-Alginate Beads for the Oral Delivery of Transforming Growth Factor-B1 (TGF-B1): Stabilization of TGF-B1 by the Addition of Polyacrylic Acid within Acid-Treated Beads. *J. Controlled Release* **1994**, *30* (3), 241.
(72) Shirakura, T.; Kelson, T. J.; Ray, A.; Malyarenko, A. E.; Kopelman, R. Hydrogel Nanoparticles with Thermally Controlled Drug Release. *ACS Macro Lett.* **2014**, *3* (7), 602.
(73) Wei, Q.; Young, J.; Holle, A.; Li, J.; Bieback, K.; Inman, G.; Spatz, J. P.; Cavalcanti-Adam, E. A. Soft Hydrogels for Balancing Cell Proliferation and Differentiation. *ACS Biomater. Sci. Eng.* **2020**, *6* (8), 4687.
(74) Zhang, J.; Zhao, R.; Li, B.; Farrukh, A.; Hoth, M.; Qu, B.; del Campo, A. Micropatterned Soft Hydrogels to Study the Interplay of Receptors and Forces in T Cell Activation. *Acta Biomater.* **2021**, *119*, 234.
(75) Mavituna, F.; Park, J. M.; Gardner, D. Determination of the Effective Diffusion Coefficient of Glucose in Callus Tissue. *Chem. Eng. J.* **1987**, *34* (1), B1.
(76) Hettiaratchi, M. H.; Schudel, A.; Rouse, T.; García, A. J.; Thomas, S. N.; Guldberg, R. E.; McDevitt, T. C. A Rapid Method for Determining Protein Diffusion through Hydrogels for Regenerative Medicine Applications. *APL Bioeng.* **2018**, *2* (2), No. 026110.
(77) Hanson, B. S.; Dougan, L. Network Growth and Structural Characteristics of Globular Protein Hydrogels. *Macromolecules* **2020**, *53* (17), 7335−7345.
(78) Hughes, M. D. G.; Cussons, S.; Hanson, B. S.; Cook, K. R.; Feller, T.; Mahmoudi, N.; Baker, D. L.; Ariëns, R.; Head, D. A.; Brockwell, D. J.; Dougan, L. Building Block Aspect Ratio Controls Assembly, Architecture, and Mechanics of Synthetic and Natural Protein Networks. *Nat. Commun.* **2023**, *14* (1), 5593.
(79) Lane, T.; Holloway, J. L.; Milani, A. H.; Saunders, J. M.; Freemont, A. J.; Saunders, B. R. Double Network Hydrogels Prepared from pH-Responsive Doubly Crosslinked Microgels. *Soft Matter* **2013**, *9* (33), 7934.
(80) Sharma, M.; de Alba, E. Assembly Mechanism of the Inflammasome Sensor AIM2 Revealed by Single Molecule Analysis. *Nat. Commun.* **2023**, *14* (1), 7975.
(81) Bryan, N. B.; Dorfleutner, A.; Kramer, S. J.; Yun, C.; Rojanasakul, Y.; Stehlik, C. Differential Splicing of the Apoptosis-

https://doi.org/10.1021/acsomega.4c06984
ACS Omega 2025, 10, 10852−10865

Associated Speck like Protein Containing a Caspase Recruitment Domain (ASC) Regulates Inflammasomes. *J. Inflamm* **2010**, *7* (1), 23.
(82) Sharma, M.; de Alba, E. Structure, Activation and Regulation of NLRP3 and AIM2 Inflammasomes. *Int. J. Mol. Sci.* **2021**, *22* (2), 872.
(83) de Alba, E. Structure and Interdomain Dynamics of Apoptosis-Associated Speck-like Protein Containing a CARD (ASC)*. *J. Biol. Chem.* **2009**, *284* (47), 32932−32941.
(84) de Alba, E. Structure, Interactions and Self-Assembly of ASC-Dependent Inflammasomes. *Arch. Biochem. Biophys.* **2019**, *670*, 15−31.
(85) Diaz-Parga, P.; de Alba, E. Inflammasome Regulation by Adaptor Isoforms, ASC and ASCb, via Differential Self-Assembly. *J. Biol. Chem.* **2022**, *298* (3), No. 101566.
(86) Diaz-Parga, P.; de Alba, E. Protein Interactions of the Inflammasome Adapter ASC by Solution NMR. *Methods Enzymol* **2019**, *625*, 223−252.
(87) Nambayan, R. J. T.; Sandin, S. I.; Quint, D. A.; Satyadi, D. M.; de Alba, E. The Inflammasome Adapter ASC Assembles into Filaments with Integral Participation of Its Two Death Domains, PYD and CARD. *J. Biol. Chem.* **2019**, *294* (2), 439−452.
(88) Gaspar-Morales, E. A.; Waterston, A.; Sadqi, M.; Diaz-Parga, P.; Smith, A. M.; Gopinath, A.; Andresen Eguiluz, R. C.; De Alba, E. Natural and Engineered Isoforms of the Inflammasome Adaptor ASC Form Noncovalent, pH-Responsive Hydrogels. *Biomacromolecules* **2023**, *24* (12), 5563.

https://doi.org/10.1021/acsomega.4c06984
ACS Omega 2025, 10, 10852−10865